NANO LETTERS

2009
Vol. 9, No. 1
279-282

Optical Absorption Enhancement in Amorphous Silicon Nanowire and Nanocone Arrays

Jia Zhu,[†] Zongfu Yu,[‡] George F. Burkhard,[‡] Ching-Mei Hsu,[§] Stephen T. Connor,[||] Yueqin Xu,[⊥] Qi Wang,[⊥] Michael McGehee,[§] Shanhui Fan,[†] and Yi Cui*[,§]

Department of Electrical Engineering, Department of Applied Physics, Department of Materials Science and Engineering, and Department of Chemistry, Stanford University, Stanford, California 94305, and National Renewable Energy Laboratory, 1617 Cole Boulevard., Golden, Colorado 80401

Received September 23, 2008; Revised Manuscript Received November 26, 2008

ABSTRACT

Hydrogenated amorphous Si (a-Si:H) is an important solar cell material. Here we demonstrate the fabrication of a-Si:H nanowires (NWs) and nanocones (NCs), using an easily scalable and IC-compatible process. We also investigate the optical properties of these nanostructures. These a-Si:H nanostructures display greatly enhanced absorption over a large range of wavelengths and angles of incidence, due to suppressed reflection. The enhancement effect is particularly strong for a-Si:H NC arrays, which provide nearly perfect impedance matching between a-Si:H and air through a gradual reduction of the effective refractive index. More than 90% of light is absorbed at angles of incidence up to 60° for a-Si:H NC arrays, which is significantly better than NW arrays (70%) and thin films (45%). In addition, the absorption of NC arrays is 88% at the band gap edge of a-Si:H, which is much higher than NW arrays (70%) and thin films (53%). Our experimental data agree very well with simulation. The a-Si:H nanocones function as both absorber and antireflection layers, which offer a promising approach to enhance the solar cell energy conversion efficiency.

Hydrogenated amorphous silicon (a-Si:H), which has many important applications including thin film transistors (TFTs), solar cells, and RFIDs, is considered to be one of the most important semiconductor materials.[1−3] The advantage of a-Si:H, over its crystalline form lies in its unique production technique, as a-Si:H thin film can be deposited by PECVD at a very low temperature (100−250 °C). This allows deposition not only on glass but also on plastic and stainless steel, making it suitable for roll-to-roll processing. Because of this, the a-Si:H solar cell is one of the most promising candidates for the new generation solar cells. The typical film thickness is around 1 μm for effective light absorption in a-Si:H thin film solar cells, which is ∼2 orders of magnitude thinner than that in single crystalline Si. However the minority carrier diffusion length is typically only 300 nm.[2] The mismatch of light absorption depth and minority diffusion length can cause either insufficient absorption or carrier collection loss. Recently Atwater[4] proposed a general scheme for addressing the mismatch of light absorption and minority carrier diffusion length by using nanowire structures. A variety of semiconductor nanowires (NWs)[5−9] have been demonstrated. However, few results have been reported regarding a-Si:H NWs or nanocones (NCs) at this time. Here we report the fabrication of vertical a-Si:H NW and NC arrays using a wafer-scale Langmuir−Blodgett assembly and etching technique, which is a scalable, IC-compatible process. We have investigated the light absorption and reflection properties of these a-Si:H nanostructures for solar cell applications.

Due to the high refractive index of a-Si:H, a large portion of incident light is reflected back from the surface of a-Si:H and thus cannot be used to generate current in solar cell devices. Quarter-wavelength transparent thin films are now the industrial standard for antireflection coatings (ARCs) for thin film solar cells like the a-Si:H solar cell.[2,3] However, this quarter-wavelength ARC is typically designed to suppress reflection at a specific wavelength and at specific angles of incidence. Several groups have demonstrated broadband reflection suppression using nanostructures,[10−17] but few technologies can be applied to the new generation thin film solar cells due to either restrictions on certain materials or complexity in the fabrication process. Without depositing any ARC, our a-Si:H nanostructures, especially a-Si:H NC arrays, provide impedance matching between a-Si:H and air

* To whom correspondence should be addressed, yicui@stanford.edu.
[†] Department of Electrical Engineering, Stanford University.
[‡] Department of Applied Physics, Stanford University.
[§] Department of Materials Science and Engineering, Stanford University.
[||] Department of Chemistry, Stanford University.
[⊥] National Renewable Energy Laboratory.

10.1021/nl802886y CCC: $40.75
Published on Web 12/10/2008

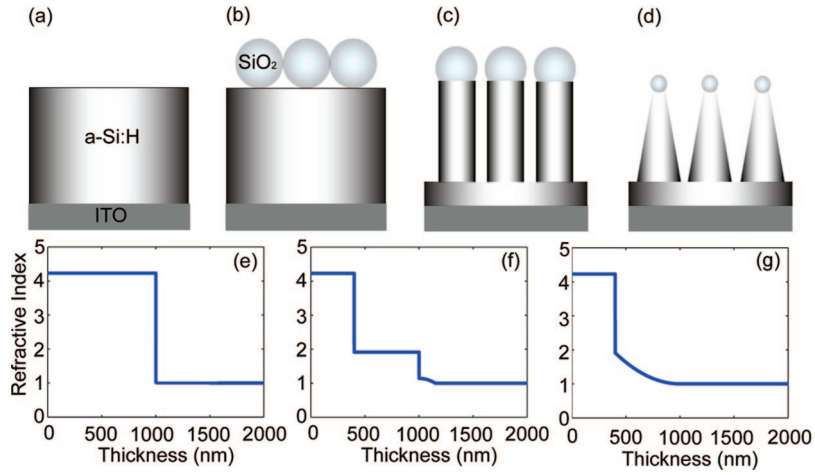

Figure 1. (a−d) Schematic illustration of 1 μm thick a-Si:H on ITO-coated glass substrate, a monolayer of silica nanoparticles on top of a-Si:H thin film, NW arrays, and NC arrays. The effective refractive index profiles of the interfaces between air and (e) a-Si:H thin film, (f) 600 nm a-Si:H NW arrays, and (g) 600 nm a-Si:H NC arrays.

through a gradual reduction of the effective refractive index. Because of the suppressed reflection, the absorption is greatly improved over a large range of wavelengths and angles of incidence.

The outline of the fabrication process for a-Si:H nanostructures is shown in Figure 1, panels a−d. A 1 μm thick a-Si:H film (Figure 1a) was grown by hot wire chemical vapor deposition (HWCVD) on an indium-tin-oxide (ITO) coated glass substrate. The Langmuir−Blodgett method was used to assemble silica nanoparticles (NPs) into a close-packed monolayer on top of an a-Si:H thin film. These silica nanoparticles (Figure 1b) were then used as an etch-mask during a chlorine-based reactive ion etching (RIE) process, since the etching rate of silica is much lower than that of a-Si:H. Either NWs (Figure 1c) or NCs (Figure 1d) can be obtained, depending on the reactive ion etching conditions.[18] The details of the etching conditions can be found elsewhere.[18] Panels e−g of Figure 1 show an effective refractive index profile calculated by averaging the refractive indices of air ($n = 1$) and a-Si:H ($n = 4.23$) weighted by volume at the interface between air and an a-Si:H thin film (Figure 1e), between air and a-Si:H NW arrays (Figure 1f), and between air and a-Si:H NC arrays (Figure 1g). The effective refractive index changes immediately from 4.23 to 1 across the flat film interface (Figure 1e), which causes the reflection of light. For a-Si:H NW arrays (Figure 1f), the refractive index of the a-Si:H NW array depends on the density of the NWs, but they always provide an intermediate refractive index step, leading to reduced reflection over a broad range of wavelengths and angles of incidence. Interestingly for the a-Si:H NC arrays, the diameter of these NCs shrinks gradually from the root to the top, resulting in a graded transition of the effective refractive index. For this reason, we expected the a-Si:H NC arrays would demonstrate the best antireflective properties and so the greatest absorption enhancement.

Three samples with a 1 μm thick a-Si:H thin film on top of ITO-coated glass were selected for the experiment. After the RIE process, the top layers of the two samples were NW and NC arrays, respectively. The third sample was left unprocessed and remained a nontextured a-Si:H thin film for use as a control. Panels a and b of Figure 2 show scanning electron microscope (SEM) images of silica nanoparticles forming a close-packed monolayer on a-Si:H thin film. These silica nanoparticles had a uniform size of about 500 nm and were close-packed and display short-range order. Panels c and d of Figure 2 show SEM images of a-Si:H NW arrays after RIE. The diameter of each NW was ~300 nm. Each nanowire was ~600 nm long. The silica nanoparticles can still clearly be seen on the top of each NW. Panels e and f of Figure 2 show SEM images of a-Si:H NC arrays. Each NC was also ~600 nm long. The tip diameter of these NCs was ~20 nm, while the base diameter was ~300 nm. It is believed that the conical shape is due to the gradual shrinkage of the size of the silica nanoparticle. After RIE, the silica nanoparticles were so small that they were no longer observable on top of NCs.

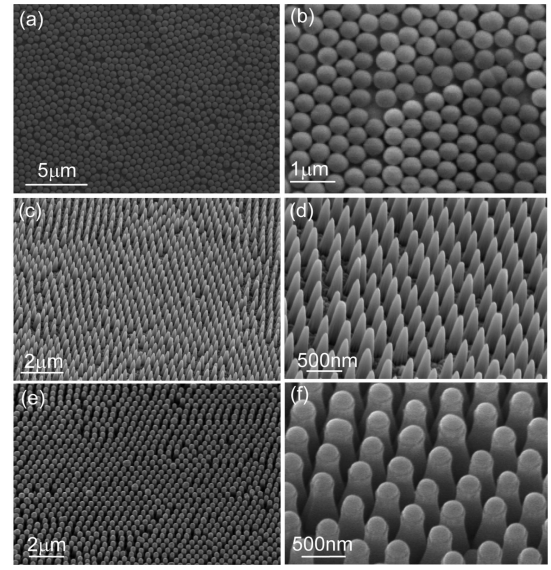

Figure 2. (a, c, e) SEM images in a large area of a monolayer of silica nanoparticles, a-Si:H NC arrays, and a-Si:H NW arrays, respectively. (b, d, f) Zoom-in SEM images of silica nanoparticles, a-Si:H NCs, and a-Si:H NWs, respectively.

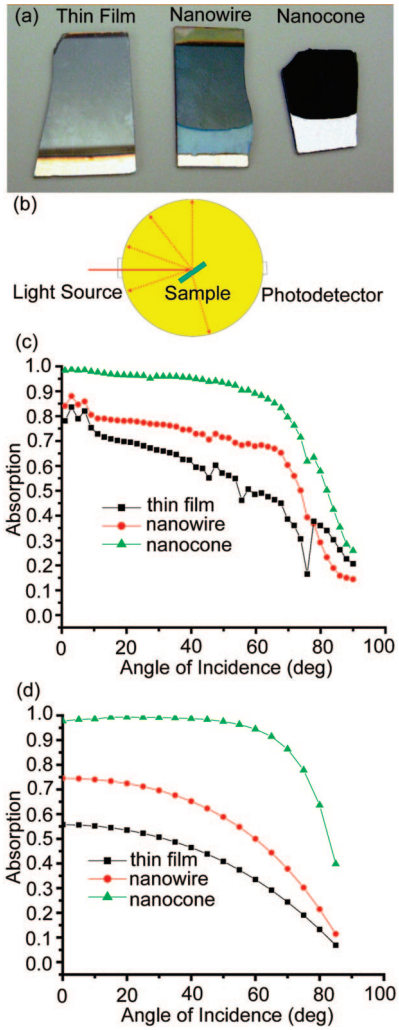

Figure 3. (a) Photographs of a-Si:H thin film (left), NW arrays (middle), and NC arrays (right). (b) Schematic illustration of hemispherical measurement using an integrating sphere (c) Measured results of absorption on samples with a-Si:H thin film, NW arrays, and NC arrays as top layer over different angles of incidence (at wavelength $\lambda = 488$ nm). (d) Simulated value of absorption on samples with a-Si:H thin film, NW arrays, and NC arrays as a top layer over different angles of incidence (at wavelength $\lambda = 488$ nm).

Figure 3a shows photographs of three samples: 1 μm thick a-Si:H thin film (left), NW arrays (middle), and NC arrays (right) with the same height as the film thickness. The thin film sample is mirror-like and highly reflective. The sample with NW arrays reflects less light while the sample with NC arrays looks black, exhibiting enhanced absorption due to suppression of reflection from the front surface. From these pictures it is obvious that, under identical conditions, the sample with NC arrays absorbed the most light, while the thin film sample reflected the most light. In order to quantitatively characterize the absorption of these samples, we carried out absolute hemispherical measurements with an integrating sphere (Labsphere). A schematic of this measurement is shown in Figure 3b. A tungsten lamp coupled to a monochromator was used for wavelength-dependent measurement and an argon ion laser with 488 nm wavelength was used to measure dependence on the angle of incidence. The sample was mounted at the center of the sphere. The reflected and transmitted light from the sample was uniformly scattered by the integrating sphere and collected by a photodetector. In our measurement, we accounted for all light reflected from and transmitted through the sample, so this can be considered a measurement of the absolute absorption. For a numerical comparison we also solved the Maxwell equation with rigorous coupled-wave analysis (RCWA) method.[19,20] This frequency-domain method allowed us to simulate the dispersive materials with tabulated dielectric constant data from experiments. The dielectric constant for a-Si:H was taken from a handbook.[21] In the simulation, a plane wave was incident on the periodic nanopatterned a-Si:H structure. The transmitted and reflected waves were calculated, from which we derived the absorption of the structures.

The total absorption of three different kinds of samples at wavelength $\lambda = 488$ nm is shown in Figure 3c for different angles of incidence. The results of the RCWA calculations are shown in Figure 3d. For the reasons we explained above, the sample with NC arrays demonstrated the highest absorption. The measured absorption of the NC sample is 98.4% around normal incidence, which agrees well with the calculated value of 97.8%. The high absorption of the NC arrays (~98%) presents a significant advantage over NW arrays (85%) and thin film (75%). As the angle of incidence increased, the total absorption decreased as total reflection increased for all the three samples, although in all cases the NC arrays showed significantly higher absorption than the NW arrays, which showed higher absorption than the thin film. At angles of incidence up to 60°, the total absorption was maintained above 90% for the NCs. This value of 90% absorption for the NCs compares favorably with 70% for the NWs and 45% for thin film. In general the simulation agrees well with our experimental data over a wide range of angles. At incident angles close to normal, small differences exist between the measured and the calculated values, and there appears to be fluctuations of the measured value for thin film and NWs. This is because, at normal incidence, some of the reflected light could escape through the port where the laser beam entered. Differences in the samples' surface roughness also contributed to the difference between experimental and simulated data.

The absorption measurement was carried out over a broad range of wavelengths (400−800 nm), which cover most of the spectrum that is useful for a-Si:H solar cells. The measured results are summarized in Figure 4a, and the calculated results are shown in Figure 4b. Between 400 and 650 nm, the absorption of the NC arrays was maintained above 93%, which is much better than the NW arrays (75%) and thin film (64%). The measured total absorption decreased to 88% at 700 nm, which corresponds to the a-Si:H band gap (1.75 eV), also better than NWs (70%) and thin films (53%). The experimental data match with simulation very well (Figure 4b). The small difference between experiment and theory near the 700 nm is mainly due to the lack of accurate parameters for simulation near the band gap of a-Si:H.

In summary, we fabricated a-Si:H NWs and NCs using a scalable and IC-compatible process. Compared with flat thin

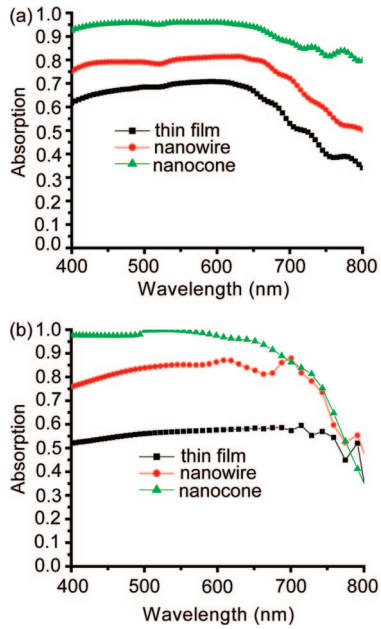

Figure 4. (a) Measured value of absorption on samples with a-Si:H thin film, NW arrays, and NC arrays as top layer over a large range of wavelengths at normal incidence. (b) Calculated value of absorption on a-Si:H thin film, NW sample, and NC sample over a large range of wavelengths at normal incidence.

film and NW arrays, the NC arrays provided excellent impedance matching between a-Si:H and air through a gradual reduction of the effective refractive index away from the surface and, therefore, exhibited enhanced absorption due to superior antireflection properties over a large range of wavelengths and angles of incidence. These novel a-Si:H NCs may be suitable for low cost, large area solar cell devices and other applications which benefit from antireflective coatings.

Acknowledgment. Y.C. acknowledges support from U.S. Department of Energy under the Award Number DE-FG36-08GOI8004. G.B. was supported by a grant from the global climate and energy project. J.Z. is a CPN Fellow.

References

(1) Carlson, D. E.; Wronski, C. R. *Appl. Phys. Lett.* **1976**, *28* (11), 671–673.
(2) Street, R. A. *Hydrogenated Amorphous Silicon*; Cambridge University Press: Cambridge, 1991.
(3) Shah, A. V.; Schade, H.; Vanecek, M.; Meier, J.; Vallat-Sauvain, E.; Wyrsch, N.; Kroll, U.; Droz, C.; Bailat, J. *Prog. Photovoltaics* **2004**, *12* (2−3), 113–142.
(4) Kayes, B. M.; Lewis, N. S.; Atwater, H. A. *J. Appl. Phys.* **2005**, *97* (11), 114302.
(5) Kelzenberg, M. D.; Turner-Evans, D. B.; Kayes, B. M.; Filler, M. A.; Putnam, M. C.; Lewis, N. S.; Atwater, H. A. *Nano Lett.* **2008**, *8* (2), 710–714.
(6) Law, M.; Greene, L. E.; Johnson, J. C.; Saykally, R.; Yang, P. *Nat. Mater.* **2005**, *4* (6), 455–459.
(7) Tian, B.; Zheng, X.; Kempa, T. J.; Fang, Y.; Yu, N.; Yu, G.; Huang, J.; Lieber, C. M. *Nature* **2007**, *449* (7164), 885–889.
(8) Garnett, E. C.; Yang, P. *J. Am. Chem. Soc.* **2008**, *130* (29), 9224–9225.
(9) Tsakalakos, L.; Balch, J.; Fronheiser, J.; Korevaar, B. A.; Sulima, O.; Rand, J. *Appl. Phys. Lett.* **2007**, *91* (23), 233117.
(10) Hu, L.; Chen, G. *Nano Lett.* **2007**, *7* (11), 3249–3252.
(11) Huang, Y.-F.; Chattopadhyay, S.; Jen, Y.-J.; Peng, C.-Y.; Liu, T.-A.; Hsu, Y.-K.; Pan, C.-L.; Lo, H.-C.; Hsu, C.-H.; Chang, Y.-H.; Lee, C.-S.; Chen, K.-H.; Chen, L.-C. *Nat. Nanotechnol.* **2007**, *2* (12), 770–774.
(12) Lee, Y. J.; Ruby, D. S.; Peters, D. W.; McKenzie, B. B.; Hsu, J. W. P. *Nano Lett.* **2008**, *8* (5), 1501–1505.
(13) Lohmuller, T.; Helgert, M.; Sundermann, M.; Brunner, R.; Spatz, J. P. *Nano Lett.* **2008**, *8* (5), 1429–1433.
(14) Wei-Lun Min, B. J. P. J. *Adv. Mater.* **2008**, *9999* (9999),
(15) Xi, J. Q.; Schubert, M. F.; Kim, J. K.; Schubert, E. F.; Chen, M.; Lin, S.-Y.; Liu, W.; Smart, J. A. *Nat. Photonics* **2007**, *1* (3), 176–179.
(16) Yang, Z. P.; Ci, L.; Bur, J. A.; Lin, S. Y.; Ajayan, P. M. *Nano Lett.* **2008**, *8* (2), 446–451.
(17) Muskens, O. L.; Gómez Rivas, J.; Algra, R. E.; Bakkers, E. P. A. M.; Lagendijk, A. *Nano Lett.* **2008**, *8* (9), 2638–2642.
(18) Ching-Mei, Hsu; Connor, S. T.; Tang, M. X.; Cui, Y. *Appl. Phys. Lett.* **2008**, *93*, 133109.
(19) Tikhodeev, S. G.; Yablonskii, A. L.; Muljarov, E. A.; Gippius, N. A.; Ishihara, T. *Phys. Rev. B* **2002**, *66* (4), 045102.
(20) Gaylord, M. G. M. a. T. K. *J. Opt. Soc. Am. A* **1986**, *3*, 1780–1787.
(21) Palik, E. D. *Handbook of Optical Constants of Solids*; Academic Press: New York, 1985.

NL802886Y